Chemical Vapor Deposition

DOI: 10.1002/cvde.200506377

Full Paper

Atomic Layer Deposition of Praseodymium Aluminum Oxide for Electrical Applications**

By *Philippe de Rouffignac* and *Roy G. Gordon**

Praseodymium aluminum oxide (PAO) thin films were grown by atomic layer deposition (ALD) from a new precursor, tris(*N*,*N*′-diisopropylacetamidinato) praseodymium, ($Pr(amd)_3$), trimethylaluminum (TMA), and water. Smooth, amorphous films having varying compositions of the general formula $Pr_xAl_{2-x}O_3$ were deposited on HF-last silicon and analyzed for physical and electrical characteristics. The films were pure according to Rutherford backscattering spectrometry (RBS) and secondary ion mass spectrometry (SIMS). The permittivity of the thin film with the stoichiometry of $Pr_{1.15}Al_{0.85}O_3$ was 18, and all annealed films displayed very low leakage currents compared to other high-*k* oxide films deposited using ALD. A leakage current density of 1.1×10^{-4} A cm^{-2} was achieved for a PAO film with an equivalent oxide thickness of 1.46 nm. Annealed films also displayed nearly zero flat-band voltage shifts and low hysteresis (< 10 mV). The optimal growth parameters and electrical properties were achieved with $Pr_{1.15}Al_{0.85}O_3$. Atomic force microscopy (AFM) determined that high temperature annealing (850 °C) had no effect on the smoothness of the films (rms of 0.17 nm).

Keywords: ALD, Praseodymium aluminum oxide, Praseodymium aluminate, Amidinate, High-κ dielectric

1. Introduction

Praseodymium aluminum oxide (PAO) could be one of the most interesting high-*k* materials that could be used in metal oxide semiconductor field-effect transistors (MOSFETs) and dynamic random access memories (DRAMs).[1] However, it has not been fully characterized as a high-*k* dielectric. To the best of our knowledge, PAO has never been deposited using either physical or CVD techniques. Praseodymium is a lanthanide, and it would be expected that the electrical characteristics would be somewhat similar to pure praseodymium oxide. In particular, praseodymium oxide has a high permittivity ($\varepsilon_r = 25$),[2] and low leakage current due to a fairly large bandgap ($E_g \approx 3.5$eV) and high, symmetrical band offsets with respect to silicon (> 1 eV).[3] It is also thermodynamically stable in contact with silicon.[3] Though the material has available *f* electrons, it has been shown to be an excellent insulator. The electrons available for conduction are thought to have very heavy electron masses and therefore very low mobility.[4]

Praseodymium oxide films have been grown by several physical methods,[3,5] by CVD,[6] and recently by using an ALD process.[7] ALD is a very attractive method for depositing advanced gate oxides and DRAM insulators, because the film thickness is easy to control, and the uniformity across the wafer and deep trenches is better than with competing deposition methods. However, ALD of praseodymium-containing oxides or aluminates has been a challenge. Using ALD, Kukli et al. deposited Pr_2O_3 from $Pr[N(SiMe_3)_2]_3$ and H_2O.[7] As with other ALD processes developed for lanthanide-based high-*k* oxides, including lanthanum oxide, yttrium oxide, and lutetium oxide,[8] the ALD of Pr_2O_3 presented some difficulties in achieving the excellent electrical properties of films made via physical vapor deposition methods. Though ALD was achieved using $Pr[N(SiMe_3)_2]_3$ and H_2O, the ligand removal was not complete. The reaction left large amounts of carbon, silicon, and hydrogen in the films. The less than ideal electrical properties of this and other ALD films are due to this relatively high impurity content of carbon, and of hydrogen in the form of trapped hydroxyls.[9] These impurities have been shown to be detrimental to device operation, especially with regard to leakage current density.[9] Though praseodymium oxide has been fabricated in various ways, there have been no reports outlining successful deposition of any PAO films using CVD or ALD.

Most ALD processes require the presence of an oxide starting surface or –OH-terminated surface. Deposition of a film without the use of an oxidized starting surface is desirable. For many applications, including use as a gate dielectric, an interlayer of a low-*k* material between the semiconductor and the high-*k* film is detrimental to performance. In some cases, growth will occur on a bare Si sur-

[*] Prof. R. G. Gordon, P. de Rouffignac
Department of Chemistry and Chemical Biology
Harvard University, Cambridge, MA 02138, (USA)
E-mail: gordon@chemistry.harvard.edu

[**] Kyoug-ha Kim is greatly acknowledged for his XRD spectra and valuable discussions. Appreciation also goes to Micron Technology for providing SIMS and XPS analysis. This work was supported in part by the National Science Foundation grant CTS-0236584.

face but during the deposition sequence the precursors used would promote interfacial layer (IL) oxide growth.[10] Previously, our group has demonstrated the successful deposition of lanthanum aluminum oxide using $La(amd)_3$ and H_2O on hydrogen-terminated silicon.[11] The praseodymium precursors used in our present study were also able to nucleate on a HF treated, hydrogen-terminated silicon surface. Growth of an IL is also inhibited during this process.

A new ALD praseodymium precursor, tris(*N*,*N*′-diisopropylacetamidinato)praseodymium, $Pr(amd)_3$ (Fig. 1), was synthesized in order to examine whether this ligand system could achieve desirable ALD properties with other lanthanide series elements. The synthesis and properties of a similar La compound have been described previously,[12]

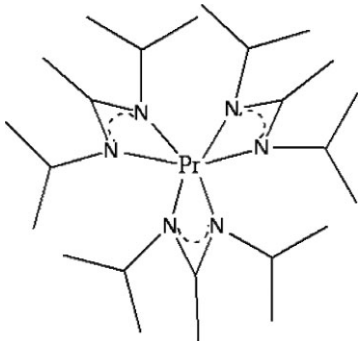

Fig. 1. Molecular formula of tris(*N*,*N*′-diisopropylacetamidinato) praseodymium, ($Pr(amd)_3$).

and it is now commercially available.[13] The synthesis of $Pr(amd)_3$ is reported for the first time in this paper. $Pr(amd)_3$ is very volatile, subliming at 95 °C with a vapor pressure of 0.04 Torr. It reacts quickly with water. One problem with using water for the ALD of praseodymium oxide is that the films tend to react with water vapor to form praseodymium hydroxides such as $Pr(OH)_3$ and PrO(OH).[14] However, these hydroxides are not thermally stable.[15] They decompose to pure oxide over time at elevated temperatures. If water is used as the oxidant during the deposition of praseodymium oxide, the film will absorb water to form the hydroxide phase mentioned above. During the purge portion of the deposition cycle, the film slowly desorbs the trapped water. During subsequent cycles, the desorbing water can react with incoming precursor, ruining the self-limiting nature of the ALD reaction. To overcome this water adsorption/desorption problem we deposited alternating layers of praseodymium oxide and aluminum oxide to form a mixed PAO film. The incorporation of aluminum oxide seems to make the film impervious to water. Fortunately, stoichiometric PAO also has electrical properties comparable with pure praseodymium oxide.

In this article, PAO films of varying praseodymium to aluminum ratios were deposited from the novel precursor using ALD. The defining characteristics of a true ALD process are examined. Analysis of the film composition, nucleation, and interface properties, and post-deposition annealing will also be used to explain observed electrical properties.

2. Results and Discussion

2.1. Deposition Parameters

Initial ALD experiments using $Pr(amd)_3$ and water in alternating cycles produced non-uniform films thicker near the gas inlet. After ruling out decomposition, it was found that extremely long purge times, on the order of several minutes, could mitigate the effect. From separate X-ray photoelectron spectroscopy (XPS) and RBS measurements it was found that the oxygen to praseodymium ratio was much higher than the 3:2 ratio that is expected for a stoichiometric Pr_2O_3 film. With that information, and the knowledge that lanthanides, including Pr, can form stable hydroxides,[16] we concluded that water was being chemisorbed during the water pulse. According to the literature,[16] PrO(OH) can be thermally dehydrated only at temperatures above 380 °C. To overcome this problem, TMA was added to the ALD process to make $Pr_xAl_{2-x}O_3$. PAO was shown to be more stable with respect to water absorption and, as mentioned earlier, also has desirable electrical properties.

The ALD sequence used to deposit $Pr_xAl_{2-x}O_3$ was: m*($Pr(amd)_3$ → 10 s purge → H_2O → 5 s purge) → 30 s purge → TMA → 10s purge → H_2O → 20 s purge, with m praseodymium and water cycles being completed before the TMA and water cycle. The overall pulse sequence is then repeated to form a multistack of sub-monolayer nanolaminates.

We have examined several different Pr precursor to TMA pulsing ratios. Table 1 shows the stoichiometry of the $Pr_xAl_{2-x}O_3$ for a given pulsing ratio as determined by RBS. The growth rate for each pulsing ratio is also provided. The saturation of the Pr precursor was also examined in order to establish that this process is self-limiting. The Pr precursor achieved saturation when at least 4 nmol cm^{-2} of pre-

Table 1: Evaluation of stoichiometry and growth rate for varying $Pr(amd)_3$ to TMA pulse ratios.

Pulse ratio Pr:Al	Stoichiometry	Growth rate of Pr component [Å per cycle]
2:1	$Pr_{0.7}Al_{1.3}O_3$	0.896
3:1	$Pr_{1.15}Al_{0.85}O_3$	0.982
4:1	$Pr_{1.55}Al_{0.45}O_3$	0.995
5:1	$Pr_{1.75}Al_{0.25}O_3$	1.031
infinite	$Pr_2O_{3.5-4}$	1.331

cursor was supplied to the reactor, and no further film growth was observed when the precursor dose was increased. TMA and water is a well known ALD reaction and is known to have a growth rate of 1.07 Å per cycle.[17] By using this growth rate, the growth rate of the Pr component of the mixed film can be estimated (Table 1). The growth rate of the Pr component is relatively constant until the Pr/Al pulsing ratio exceeds 3:1. For ratios in excess of 3:1 the growth rate of the Pr component, as a function of cycle number, becomes nonlinear (not shown). Nonlinearity is an indicator of non-self-limiting surface reactions so can no longer be considered ALD. The hydroxyl groups that remain under these conditions also severely reduce electrical performance by increasing the leakage current. It is possible to return to a linear growth mechanism provided the purge times after the water pulse are lengthened; however the purge times become unacceptably long. This puts an upper bound to the Pr to Al pulse ratio that provides a true ALD process and minimizes impurities. The pulse ratio of 3 Pr to 1 Al provides the closest stoichiometry to bulk PAO and was chosen to be characterized more fully. All the following conclusions and data correspond to the 3:1 Pr to Al ratio.

The thickness vs. cycle number can be seen in Figure 2. The film grows linearly with cycle number, and the inhibition period on HF-last silicon is quite small for an ALD process. The inhibition corresponds to 1 cycle for the 3:1

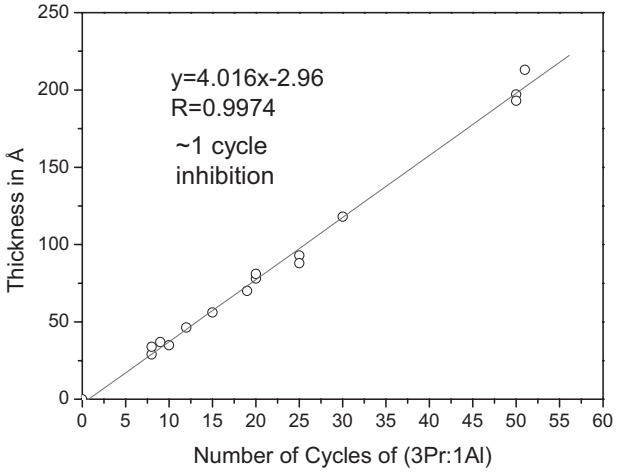

Fig. 2. Thickness as a function of cycle number for $Pr_{1.15}Al_{0.85}O_3$. Growth rate is linear and inhibition is low (1 cycle) in HF-last Si.

pulse ratio. The growth rate derived from this plot is also relatively rapid if we consider the large ligand size required to form this volatile praseodymium compound. Not shown, but equally important for ALD, is the spatial uniformity of the deposition. Many applications benefit from having high spatial uniformity (one of the defining characteristics of ALD) which, in this case, averages ±4.5 % across a 25 cm deposition zone.

2.2. Film Structure

The refractive index of the as-deposited material with a composition of $Pr_{1.15}Al_{0.85}O_3$ was determined to be 1.80 for thick films. The stoichiometry of $Pr_{1.15}Al_{0.85}O_3$ for the 3:1 pulse ratio was derived from RBS measurements. Neither carbon nor nitrogen were detected (< 1 at.-%) in RBS spectra taken using glassy carbon as the substrate. To get another estimate of its purity, a 20 nm film was measured using XPS depth profiling by argon ion sputtering (not shown). Carbon, sulfur, and fluorine were determined by XPS to be present at levels below 1 %. The concentration of carbon agrees with the limit found using RBS. Lithium and chlorine levels were measured using SIMS. These atoms are of particular concern because they are present in the synthesis of the Pr precursor used. In earlier, unpublished work on PAO nanolaminates, the precursor used was not fully purified, and lithium and chlorine were subsequently found in a deposited film. After refining the purification process for $Pr(amd)_3$ using a second sublimation step, the PAO films showed levels of lithium and chlorine below the detection limit (< 0.7 %) of SIMS. This low level of various ion impurities should not introduce significant amounts of mobile or fixed charge which can be detrimental to the electrical properties.

Another characteristic of ALD is its ability to coat high aspect ratio features conformally. In order for the process to achieve this conformality, it is necessary to have a high exposure of all of the precursors to the surface. This can be accomplished in several ways. The exposure is determined by the amount of precursor that resides over a given feature for a given amount of time. In a flow reactor, the time constant is set by the pumping speed, and the amount of precursor is determined by the vapor pressure and gas volume of precursor being delivered, so the exposure can be increased by increasing any one of these parameters. One of the most effective means of increasing the exposure is to trap the precursor above the substrates for a short amount of time (of the order of a few seconds). Typical gas residence times in our flow reactor are 10–100 ms. By increasing to a few seconds the time the precursor resides in the deposition chamber, we increased exposure by a factor of 100 or more. The aspect ratio that can be achieved by a given ALD process is proportional to the square root of the exposure,[18] providing, in this case, an increase of ten times the aspect ratio normally achieved. Figure 3 shows a picture of a normal, fused silica capillary tube that has had 350 Å of $Pr_{1.15}Al_{0.85}O_3$ deposited using an exposure of the precursor of 2×10^5 Langmuir. The interface between the higher refractive index PAO and the silica becomes visible when the capillary tube is filled with index fluid (SPI supplies $n_d = 1.460$) that has the same refractive index as the tube. The capillary tube has an internal diameter of 20 μm, and the film penetrates 590 μm into the tube on both sides. This translates to an aspect ratio of almost 30:1. The drawback of this technique is that it is difficult to determine if

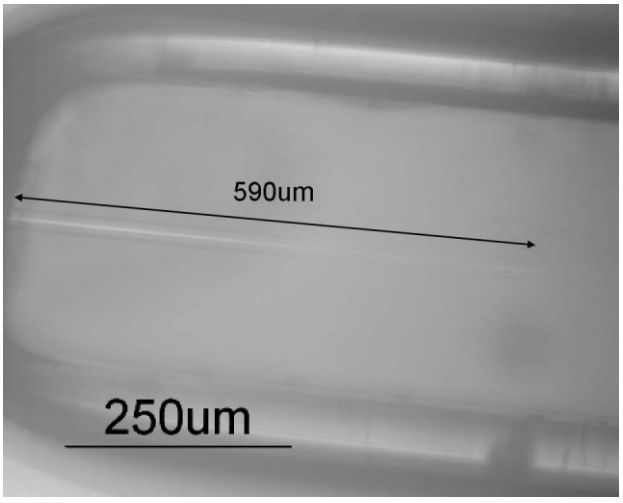

Fig. 3. Optical microscope image (20×) of a silica capillary tube with 35 nm of PAO deposited 590 mm down the 20 mm opening. Penetration is independent of tube orientation to the precursor flow direction.

the penetrated film is 100 % conformal on the side walls of the capillary tube. Further experiments will be performed to ascertain the actual conformality. An aspect ratio of 30:1 is somewhat lower than that achieved by other ALD processes using the same ligand system, but it should be noted that the exposure of the precursor was lower in this case. Given a higher exposure, a higher aspect ratio can probably be achieved.

The films are very smooth. Figure 4a shows a 5 μm × 5 μm AFM scan of a 36nm PAO film deposited on HF-last silicon. The film was annealed at 600 °C for 5 min under nitrogen at atmospheric pressure, and later aggressively annealed at 850 °C for 30 min under nitrogen at a pressure of 300 mTorr. The scan shows a very smooth film. The rms roughness of the film was determined to be 0.17 nm, which is approximately the same as that of the bare substrate. This low level of roughness is due to an amorphous structure and to high nucleation density uniformly distributed across the substrate, along with a layer-by-layer growth mode. The glancing angle X-ray diffraction (XRD) taken of the same substrate indicates an amorphous film for both the low and high temperature anneals (Fig. 4b).

2.3. Electrical Characterization

As a candidate for gate dielectrics, DRAM capacitor applications, and other advanced semiconductor devices, it is important to accurately quantify the electrical properties of the material. Figure 5a shows a graph of equivalent oxide thickness (EOT) as a function of physical thickness. The EOT was determined by simulating an ideal silicon oxide capacitance-voltage (C–V) curve for each film using the Hauser simulation program.[19] The slope of the plotted data provides the dielectric constant, and the y-intercept provides the thickness of the IL. For the $Pr_{1.15}Al_{0.85}O_3$ films as-deposited on HF-last Si at 295 °C, the dielectric constant is 17.7 and the thickness of the IL is about 5 ± 1 Å. The films were subsequently annealed in forming gas at 400 °C for 30min. The resulting capacitance data for these films indicates a slight reduction in dielectric constant to 16.1 and an IL of 4 ± 1 Å. The slight reduction in dielectric constant without an increase in the thickness of the IL is not typically seen in high-k dielectrics. We believe the annealing step removes some trapped hydroxyls present in the as-deposited film. Hydroxyls can cause small increases in the dielectric constant at low frequencies, but can also be a source of fixed charges. Figure 5b is a graph of the flatband voltage (V_{fb}) as a function of the physical thickness. The slope of this plot can be used to extract the amount of fixed charge, Q_f, in the film. For the as-deposited film the Q_f is $+1 \times 10^{13}$ cm^{-2}, and for the annealed film it is -6.4×10^{11} cm^{-2}. The forming gas anneal reduces the fixed charge by a factor of 15 and also switches the sign of the fixed charge from positive to negative. The presence of $(OH)^-$ in the film could account for the negative shift ($+Q_f$)

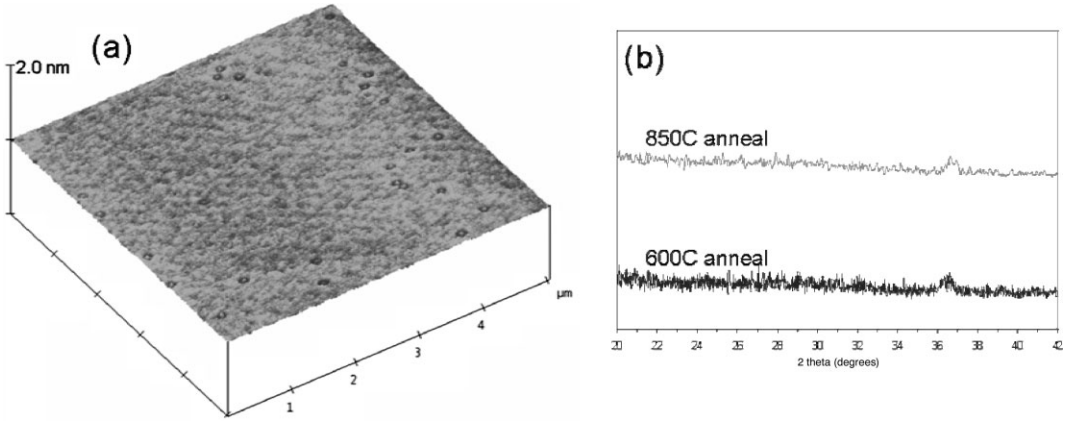

Fig. 4. a) AFM scan (5 μm × 5 μm) of a 35 nm PAO film annealed at 850 °C for 30min, rms roughness is 0.17 nm. b) Glancing angle XRD spectrum of the same 35 nm film. Note: The lone peak at 35.5° does not match any known peaks of $Pr_xAl_yO_z$, Pr_xO_y, Al_2O_3, or Si; currently under investigation

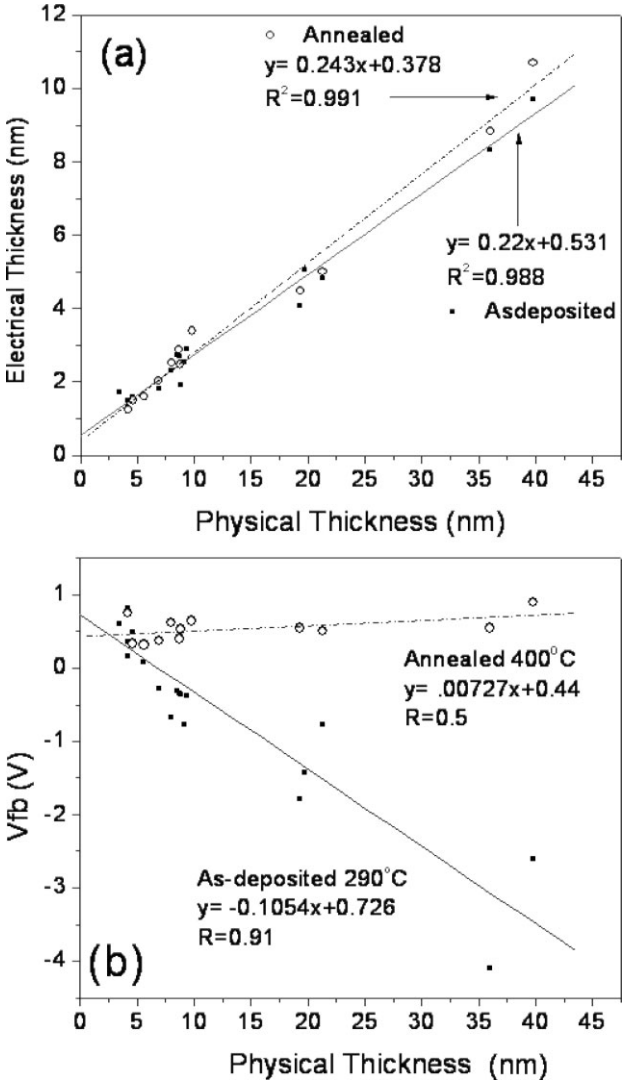

Fig. 5. a) EOT vs. physical thickness. Dielectric constant of as-deposited film is 17.7 while that of the annealed film is 16.1. Extrapolated interlayer thickness is 0.5 nm as-deposited, and 0.4 nm after anneal. b) Flat-band voltage as a function of the physical thickness. Annealing at 400 °C in N_2/H_2 (90:10) gas mixture significantly reduces the fixed charge.

seen in the as-deposited films.[20] The removal of trapped hydroxyl groups by the forming gas anneal would remove the contribution of positive trapped charge from the film. The negative Q_f found in the annealed films can be attributed to the Al atoms which act as negative charge traps.[21] Figure 6 shows a *C–V* curve for a 19.3 nm film before and after anneal. The anneal reduced the accumulation capacitance, but improved (reduced) both the V_{fb} and the hysteresis. The V_{fb} of the annealed film goes to a slightly positively shifted value of 0.51 V and the hysteresis is only 4 mV. The EOT for the annealed film is 4.375 nm, giving a dielectric constant of 17. The annealed film has a leakage current density (J) at 1 MV cm^{-1} below the measurable level, while at 2 MV cm^{-1} it is 1.7×10^{-7} A cm^{-2}. The breakdown field for this film is 4.5 MV cm^{-1}.

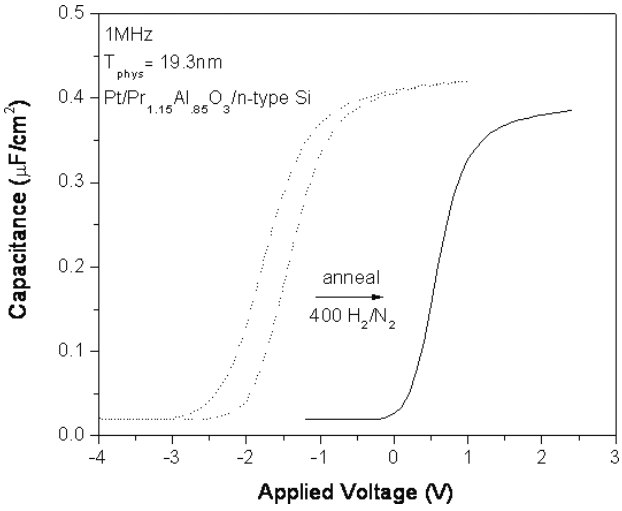

Fig. 6. *C–V* curves for an as-deposited and annealed 19 nm PAO film.

Achieving a very low EOT while maintaining low leakage current densities is a challenge for vapor-deposition techniques. In Figure 7, a *C–V* curve and *I–V* curve (inset) are shown. The *C–V* curve is that of an annealed 4.6 nm PAO film deposited on hydrogen-terminated silicon. The V_{fb} and hysteresis are very near ideal, and the accumulation capacitance achieved translates to an EOT of 1.5 nm. The inset *I–V* curve shows J plotted as a function of the V_{fb} compensated gate voltage. At 1V (V_g–V_{fb}) the leakage current density was measured to be 1.1×10^{-4} A cm^{-2}. To our knowledge, this is the lowest value of J for a 1.5 nm EOT PAO film reported in the literature. The dielectric breakdown occurs at a high field, 7.8 MV cm^{-1}. Figure 8 shows how the leakage current density varies with the EOT. The values are taken at a gate voltage of 1V. These J values are

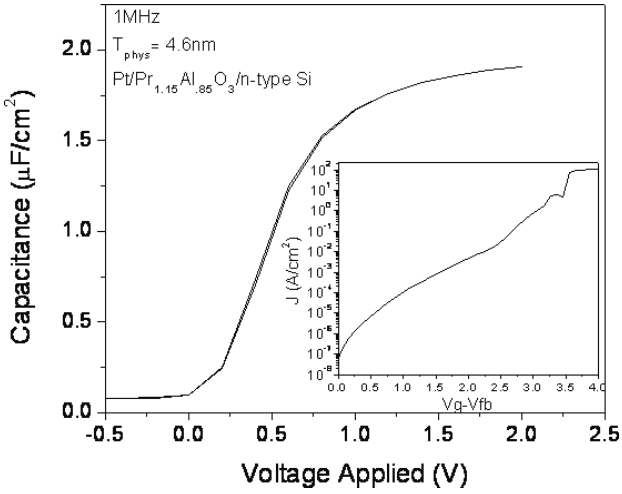

Fig. 7. *C–V* curve for an annealed 4.6 nm PAO film. The EOT is 1.5 nm. Inset: Leakage current density as a function of the applied voltage, adjusted for the flat band voltage. J at 1 V is 1×10^{-4} A cm^{-2}.

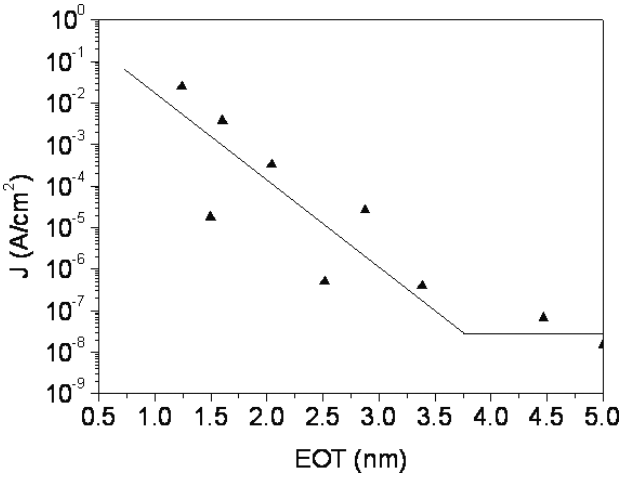

Fig. 8. Leakage current, J as a function of EOT for annealed PAO films.

over 1000 times lower than those of the equivalent SiO_2 films. These properties make PAO film, produced using ALD, a promising candidate for a gate dielectric in advanced CMOS devices. This material is also highly suitable for DRAM applications. The leakage current densities for such a low EOT surpass the requirements for next generation DRAMs.[22]

3. Conclusions

In conclusion, smooth, amorphous, and uniform PAO films were deposited by ALD. Because of the low inhibition on HF-last Si and the thin IL, it is possible to make high-quality, low-EOT PAO films using the novel precursor $Pr(amd)_3$. Purity plays a large role in determining whether the film exhibits electrical properties similar to those obtained from films deposited using physical vapor deposition methods. In this case, high purity of the praseodymium precursor and good nucleation on the HF-last silicon surface allow the production of a high-quality, conformal dielectric material.

4. Experimental

The praseodymium acetemidinate precursor was synthesized from $PrCl_3$ (anhydrous) and lithium *N*,*N*′-diisopropylacetamidinate [13] by the following method. A slurry of $PrCl_3$ in THF was mixed with lithium *N*,*N*′-diisopropylacetamidinate in ether at room temperature. The suspension was stirred overnight (12 h). The green suspension was filtered to remove the precipitated solid LiCl salt. The excess solvent was removed, and the resulting solid was purified using sublimation. The material sublimed at 85 °C under a pressure of 0.04 Torr. The melting point could not be detected below 220 °C. Figure 1 shows the chemical structure of the $Pr(amd)_3$ precursor.

The films were deposited in a flow-type reactor operated under 0.3 torr [23]. The Pr precursor was kept at 125 °C, and the TMA (Aldrich, 99.9999 %) and water (ultrahigh purity) at room temperature. The carrier gas was nitrogen purified to < 1 ppb of H_2O and O_2. A saturating dose was used for all precursors. The growth temperatures were 200–315 °C. No self-decomposition of the praseodymium precursor was observed on substrates below 315 °C. Self-decomposition was detected at $T > 315$ °C by noting that the thickness was larger close to the gas entrance to the reactor. The films were deposited from a varying number of cycles of $Pr(amd)_3$ and water, and then 1 cycle of TMA and water. This mixed nanolaminate structure was repeated from 10–100 times to produce films with thicknesses in the range 40–400 Å. Film thickness and refractive index were determined using a Rudolph Research Auto El-II ellipsometer at a wavelength of 632.8 nm with the incident angle set at 70°. RBS (General Ionics Model 4117, 1.7 MeV Tandetron) and XPS (Surface Science Lab SSX-100, and Micron Technology) were used to analyze the composition and binding structure of the PAO films. XRD, using a Scintag Model XDS 2000 with copper Ka radiation (1.54 nm wavelength), was carried out to measure crystallinity. AFM was used to measure the smoothness of the annealed films. Electrical properties (*I*–*V* and *C*–*V*) were measured on Pt/$Pr_xAl_{2-x}O_3$/n-type Si (0.05 Ω cm) MOS structures using a Signatone probe station, an HP 4275a LCR meter, and a Keithley 2400 source meter. The dot size was 1.05×10^{-3} cm^2 or 5.6×10^{-4} cm^2 as determined by scanning electron microscopy (SEM) using a standard SiO_2 MOS structure. After deposition of thin films, the back of the substrates were treated with a 10 % HF solution for 30 s to remove $Pr_xAl_{2-x}O_3$ and SiO_2. Pt was sputtered onto the bare Si to form the back contact.

Received: February 14, 2005
Final version: September 6, 2005

[1] A. I. Kingon, J.-P. Maria, S. K. Streiffer, *Nature* **2000**, *406*, 1032.
[2] R. Lo Nigro, V. Raineri, C. Bongiorno, R. Toro, G. Malandrino, I. L. Fragalà. *Appl. Phys. Lett.* **2003**, *83*, 129.
[3] A. Fissel, H. J. Osten, E. Bugiel, *J. Vac. Sci. Technol., B.* **2003**, *21*, 1765.
[4] H. J. Osten, J. P. Lui, H. J. Müssig, *Appl. Phys. Lett.* **2002**, *80*, 297.
[5] a) H. J. Osten, J. P. Liu, E. Bugiel, H. J. Müssig, P. Zaumseil, *Mater. Sci. Eng. B.* **2001**, *87*, 297. b) H. J. Osten, J. P. Liu, E. Bugiel, H. J. Müssig, P. Zaumseil, *J. Cryst. Growth.* **2002**, *235*, 229. c) H. J. Osten, J. P. Liu, H. J. Müssig, P. Zaumseil, *Microelectron. Reliab.* **2001**, *41*, 991.
[6] H. C. Aspinall, J. Gaskell, P. A. Williams, A. C. Jones, P. R. Chalker, P. A. Marshall, J. F. Bickley, L. M. Smith, G. W. Critchlow, *Chem. Vap. Deposition* **2003**, *9*, 235.
[7] K. Kukli, M. Ritala, T. Pilvi, T. Sajavaara, M. Leskelä, A. Jones, H. Aspinall, D. Gilmer, P. Tobin, *Chem. Mater.* **2004**, *16*, 5162.
[8] G. Scarel, E. Bonera, C. Wiemer, G. Tallarida, S. Spiga, M. Fanciulli, I. L. Fedushkin, H. Schumann, Yu. Lebedinskii, A. Zenkevich, *Appl. Phys. Lett.* **2004**, *85*, 630.
[9] K. Kukli, M. Ritala, M. Leskalä, T. Sajavaara, J. Keinonen, A. C. Jones, J. L. Roberts, *Chem. Vap. Deposition* **2003**, *9*, 315.
[10] M. Frank, Y. J. Chabal, M. L. Green A. Delabie, B. Brijs, G. D. Wilk, M. Y. Ho, E. B. O. da Rosa, I. J. R. Baumvol, F. C. Stedile, *Appl. Phys. Lett.* **2003**, *83*, 740.
[11] B. S. Lim, A. Rahtu, P. de Rouffignac, R. G. Gordon, *Appl. Phys. Lett.* **2004**, *84*, 3957.
[12] B. S. Lim, A. Rahtu, R. G. Gordon, *Inorg. Chem.* **2003**, *42*, 7951.
[13] Private communication from Dr. Marek Boleslawski, mboleslawski@-sial.com, at the Sigma-Aldrich Chemical Company.
[14] R. Alvero, A. Bernal, I. Carrizosa, J. A. Odriozola, J. M. Trillo, *J. Mater. Sci.* **1987**, *22*, 1517.
[15] M. D. Krasil'nikov, I. V. Vinokurov, *Izv. Akad. Nauk SSSR, Neorg. Mater.* **1979**, *15*, 483.
[16] D. F. Mullica, W. O. Milligan, G. W. Beall, *J. Inorg. Nucl. Chem.* **1979**, *41*, 525.
[17] M. Groner, J. Elam, F. Fabreguette, S. M. George, *Thin Solid Films* **2002**, *413*, 186.
[18] R. Gordon, D. Hausmann, E. Kim, J. Shepard, *Chem. Vap. Deposition.* **2003**, *9*, 73.
[19] J. R. Hauser, K. Ahmed, in *Characterization and Metrology for ULSI Technology*, (Ed: D. G. Seiler), AIP, New York **1998**.
[20] K.–J. Choi, W.-C. Shin, S.-J. Yoon, *J. Electrochem. Soc.* **2002**, *149*, F18.
[21] J. Lee, K. Koh, N. Lee, M. Cho, Y. Kim, J. Jeon, K. Cho, H. Shin, M. Kim, K. Fujihara, H. Kang, J. Moon, *Tech. Dig.-Int. Electron Devices Meet.*, IEEE, Piscataway, NJ **2000**, p.645.
[22] Semiconductor Industry Association International Technology Roadmap for Semiconductors (2004), http://public.itrs.net/ (accessed February 2006).
[23] J. S. Becker, R. G. Gordon, *Appl. Phys. Lett.* **2003**, *82*, 2239.

